Anisotropy of the in-plane g-factor of electrons in HgTe quantum wells

G. M. Minkov,[1,2] V. Ya. Aleshkin,[3,4] O. E. Rut,[1] A. A. Sherstobitov,[1,2] S. A. Dvoretski,[5] N. N. Mikhailov,[5,6] and A. V. Germanenko[1]

[1]*School of Natural Sciences and Mathematics, Ural Federal University, 620002 Ekaterinburg, Russia*
[2]*M. N. Miheev Institute of Metal Physics of Ural Branch of Russian Academy of Sciences, 620137 Ekaterinburg, Russia*
[3]*Institute for Physics of Microstructures RAS, 603087 Nizhny Novgorod, Russia*
[4]*Lobachevsky University of Nizhny Novgorod, 603950 Nizhny Novgorod, Russia*
[5]*Institute of Semiconductor Physics RAS, 630090 Novosibirsk, Russia*
[6]*Department of Physics, Novosibirsk State University, Novosibirsk 630090, Russia*

(Received 20 August 2019; revised manuscript received 4 February 2020; accepted 5 February 2020; published 24 February 2020)

The results of experimental studies of the Shubnikov–de Haas (SdH) effect in the (013)-HgTe/$Hg_{1-x}Cd_xTe$ quantum wells (QWs) of electron type of conductivity both with normal and inverted energy spectrum are reported. Comprehensive analysis of the SdH oscillations measured for the different orientations of magnetic field relative to the quantum well plane and crystallographic exes allows us to investigate the anisotropy of the Zeeman effect. For the QWs with inverted spectrum, it has been shown that the ratio of the spin splitting to the orbital one is strongly dependent not only on the orientation of the magnetic field relative to the QW plane but also on the orientation of the in-plane magnetic field component relative to crystallographic axes laying in the QW plane that implies the strong anisotropy of in-plane g-factor. In the QW with normal spectrum, this ratio strongly depends on the angle between the magnetic field and the normal to the QW plane and reveals a very slight anisotropy in the QW plane. To interpret the data, the Landau levels in the tilted magnetic field are calculated within the framework of four-band kP model. It is shown that the experimental results can be quantitatively described only with taking into account the interface inversion asymmetry.

DOI: 10.1103/PhysRevB.101.085305

I. INTRODUCTION

Spin-dependent effects in transport, tunneling, optical phenomena are interesting and important not only for understanding the role of these effects in all phenomena [1] but also for possible application. These effects are largely determined by the g-factor and its anisotropy, that is, by its dependence on the direction of the magnetic field relative to the two-dimensional plane and crystallographic axes. The g-factor anisotropy can be very strong and important in two-dimensional (2D) structures based on materials with a large spin-orbit interaction, a complex spectrum, and in the structures grown on substrates with a low-symmetric surface. The quantum wells based on the mercury cadmium telluride, $Hg_{1-x}Cd_xTe$, zinc-blende compounds belong to such a type of structures.

The energy spectrum of HgTe quantum wells (QWs) is complicated and depends strongly on the quantum well width (d). For $d < d_c \simeq 6.3$ nm, the conduction band is formed from electron states and the states of the light hole [2–8]. This type of the spectrum is named normal. At $d > d_c$, the conduction band is formed from heavy-hole states and such type of the spectrum is named "inverted." At $d = d_c$, the linear in quasimomentum (k) gapless spectrum is realized. Experimentally, the g-factor and its anisotropy was investigated in the structures both with normal and with "inverted" spectrum grown on substrates of different orientations [9–13]. In all the cases it was assumed that the in-plane g-factor ($g_\parallel$) is isotropic.

In this paper, we study the angle dependencies of the amplitude of the Shubnikov–de Haas (SdH) oscillations in tilted magnetic fields in (013)-HgTe QWs with both types of energy spectrum. We show that the ratio of the spin to orbit splitting is strongly anisotropic and this anisotropy is strongly different for QWs with $d > d_c$ and $d < d_c$. Especially, it concerns the anisotropy of in-plane g-factor. The paper is organized as follows. The samples and experimental conditions are described in the next section. The experimental results and their analysis for the QW of $d = 10$ nm with "inverted" energy spectrum are presented in Sec. III. The surprising finding is that the oscillation picture in the tilted magnetic field is strongly different for the two cases when the in-plane component changes its direction on the angle of 180°. It points to the strong anisotropy of the in-plane g-factor. In Sec. IV we describe theoretical model allowing us to calculate the spectrum of the Landau levels (LLs) in the tilted magnetic field. Comparison of the data for the QW with $d > d_c$ with theoretical results is performed in Secs. V and VI. The data obtained for QW with $d < d_c$ are inspected and analysed in Sec. VII. Section VIII is devoted to the conclusions.

II. EXPERIMENTAL

Our samples with the HgTe quantum wells were realized on the basis of HgTe/$Hg_{1-x}Cd_xTe$ heterostructures grown by the molecular beam epitaxy on a GaAs substrate with the (013) surface orientations [14]. The samples were mesa etched

TABLE I. The parameters of the $HgTe/Hg_{1-x}Cd_xTe$ heterostructures under study.

Number	Structure	d (nm)	x	n ($V_g = 0$) (cm^{-2})
1	150224	10.0	0.52	1.15×10^{11}
2	150220	4.6	0.54	1.60×10^{11}

into standard Hall bars of 0.5 mm width and the distance between the potential probes was 0.5 mm. To change and control the carrier density in the quantum well, the field-effect transistors were fabricated with parylene as an insulator and aluminium as a gate electrode. Three heterostructures with the inverted energy spectrum ($d > d_c$) and the two ones with the normal spectrum ($d < d_c$) were measured. For each heterostructure, several samples were fabricated and studied. The results for heterostructures of each type were mostly analogous; therefore, we restrict our presentation to two heterostructures listed in the Table I.

The measurements of the longitudinal (ρ_{xx}) and Hall (ρ_{xy}) resistivity were carried out using the dc technique in the linear regime of response at $T = 4.2$ K within magnetic field range 0–6 T. Note that the ρ_{xx} vs. B dependencies did not depend on the signs of the magnetic field and the dc current.

The ratio of the spin splitting (Δ_s) to the orbital one (Δ_o) $X = \Delta_s/\Delta_o$ was obtained by means of modified coincidence method [15–18]. The measurements were taken in two configurations which are shown in Fig. 1. In the first configuration, which is widely used be experimentalists, the rotation axis is perpendicular to the magnetic field and lies in the 2D plane [Fig. 1(a)]. In the second configuration, the rotator and the sample are oriented in such a way that the axis of rotation is normal to the 2D plane and tilted relative to the magnetic field [see Fig. 1(b)]. This allowed us to investigate the in-plane anisotropy of spin-to-orbit splitting ratio.

III. TILT-ANGLE DEPENDENCE OF SdH OSCILLATIONS, $d > d_c$

Let us begin with analysis of the results obtained in the first configuration. The rotation on the angle θ, as shown in Fig. 1(a), changes the ratio between the normal and in-plane components ($B_\perp$ and $B_\parallel$, respectively) of magnetic field; $B_\perp = B\cos\theta$, $B_\parallel = B\sin\theta$, where B is the total magnetic field. If we assume that the spin splitting is proportional to the total magnetic field $\Delta_s \propto B$ and the orbital splitting is proportional to the normal component $\Delta_o \propto B_{\rm perp}$, then the angle dependence of the oscillation amplitude in the low magnetic fields in which the spin splitting of oscillations is not resolved looks as follows [16,17,19]:

$$\frac{A(\theta)}{A(0)} = \frac{\cos[\pi X(\theta)]}{\cos[\pi X(0)]}, \tag{1}$$

where

$$X(\theta) = \frac{\Delta_s}{\Delta_o(\theta)} = \frac{g\mu_B B}{(e\hbar B_\perp/m)} \tag{2}$$

with μ_B as the Bohr magneton and m as effective mass. If the g-factor is anisotropic, then the spin splitting of the LL becomes angle dependent as well. In the simplest case it can be written as follows:

$$g(\theta) = \sqrt{g_\perp^2\cos(\theta)^2 + g_\parallel^2\sin(\theta)^2}, \tag{3}$$

and then

$$X(\theta) = \frac{\Delta_s(\theta)}{\Delta_o(\theta)} = \frac{m}{m_0}\frac{1}{2\cos\theta}\sqrt{g_\perp^2\cos(\theta)^2 + g_\parallel^2\sin(\theta)^2}. \tag{4}$$

So the measurements of the SdH oscillation amplitude at fixed $B_\perp$ as a function of tilt angle θ give, in principle, a possibility to find the ratio of the spin splitting to the orbital one and to obtain the g-factor value.

This method is valid when (i) $B_\perp$ is significantly less than the field of the onset of the quantum Hall effect (QHE); (ii) the amplitude of the oscillations is small so that the oscillations of the Fermi energy are negligible; and (iii) the SdH oscillations are spin-unsplit.

In this section we analyze the results obtained for the structures 1 with "inverted" spectrum ($d = 10$ nm). In Fig. 2(a), we present the magnetic field dependences of ρ_{xx} and ρ_{xy} measured at $\theta = 0$ for the electron density $n = 2.07 \times 10^{11}$ cm^{-2}. As seen the amplitude of ρ_{xx} oscillations is less than 10% and ρ_{xy} linearly depend on B (the steps of OHE are absent). This means that the oscillations of the Fermi energy within this magnetic field range can be neglected. The electron density found from the period of oscillations in $B < 0.7$ T under the

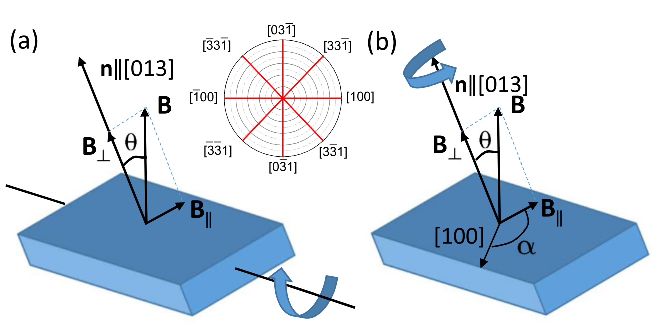

FIG. 1. Two configurations in which the angle dependencies were measured. The inset shows the crystallographic exes laying in the (013) QW plane.

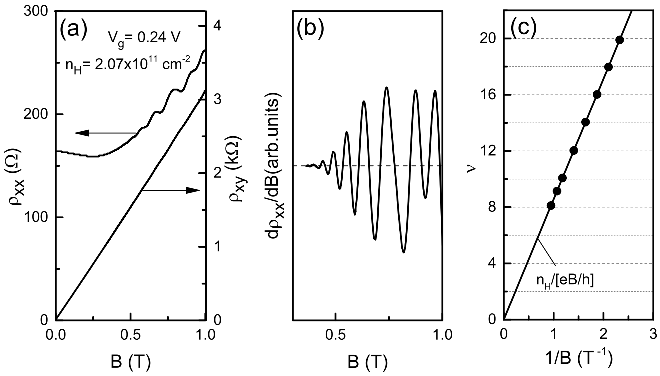

FIG. 2. The magnetic field dependencies of ρ_{xx}, ρ_{xy} (a) and the oscillations of $d\rho_{xx}/dB$ (b). (c) The dependence of the filling factor ν on positions of the ρ_{xx} minima in the reciprocal magnetic field. $\theta = 0$.

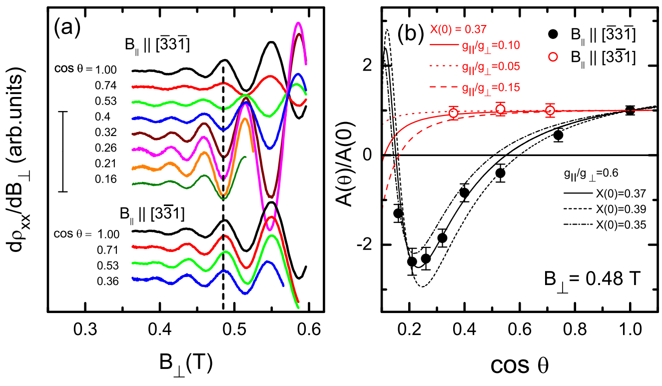

FIG. 3. (a) The dependencies $d\rho_{xx}(B_\perp)/dB_\perp$ for some angles θ, when the in-plane component appears in the directions $[\bar{3}3\bar{1}]$ and $[3\bar{3}1]$. (b) The angle dependencies of the oscillation amplitude measured at $B_\perp = 0.48$ T (symbols) and calculated as described in the text (curves). The scale shown in the panel (a) by the vertical bars is the same as in Fig. 6(a). Structure 1, $n = 2.07 \times 10^{11}$ cm^{-2}.

assumption that the Landau levels are twofold degenerate coincides with the Hall density $n_H = -1/eR_H$. So the conditions of applicability of Eq. (1) are met.

Let us now inspect the SdH oscillations in more detail. To remove the monotonic part we plot in Fig. 1(b) the dependence $d\rho_{xx}(B)/dB$. One can see that the oscillations which appear at $B \simeq 0.3$ T start to split at $B \simeq 0.7$ T. To understand the degeneracy of the Landau levels with which the observed oscillations are associated, it is instructive to consider the filling factor $\nu = n_H/(eB_{\min}/h)$ plotted against $1/B_{\min}$, where $B_{\min}$ is magnetic fields at which the minima in $\rho_{xx}(B)$ are observed. Such a dependence is represented in Fig. 2(c). It is evident that for $1/B > 1.2$ T^{-1}, $\nu > 10$ the filing factor changes by two and takes the even values therewith. This is a clear indication of the fact that the oscillations for these ν are associated with the pairwise merged Landau levels which are two spin sublevels with the same orbital number. Thus we infer that the spin splitting Δ_s is less than half the orbital splitting Δ_o, i.e., $X(0) = \Delta_s/\Delta_o < 0.5$.

Let us now consider the oscillations in tilted magnetic fields. The dependencies of the $d\rho_{xx}/dB_\perp$ on the normal to 2D plane magnetic field $B_\perp$ for the case when the in-plane component appears in directions $B_\parallel \upuparrows [\bar{3}3\bar{1}]$ and $B_\parallel \upuparrows [3\bar{3}1]$ are shown in Fig. 3(a) for some tilt angles. It is seen that the positions of the oscillations in $B_\perp$ are independent of θ within the experimental accuracy, while the amplitude of the oscillations varies significantly.

The angle dependencies of the normalized oscillation amplitude $A(\theta)/A(0)$ at $B_\perp = 0.48$ T are represented in Fig. 3(b) [20]. The negative sign of $A(\theta)/A(0)$ corresponds to jump of the oscillation phase on π. Particularly striking is that the angle dependencies of oscillation amplitudes are drastically different for $B_\parallel \upuparrows [\bar{3}3\bar{1}]$ and $B_\parallel \upuparrows [3\bar{3}1]$. The amplitude immediately decreases with the $\cos\theta$ decrease when $B_\parallel \upuparrows [\bar{3}3\bar{1}]$ and does not practically depend on θ when $B_\parallel \upuparrows [3\bar{3}1]$ within the actual θ range. All this indicates that the in-plane g-factor $g_\parallel$ differs dramatically for two opposite crystallographic directions $[\bar{3}3\bar{1}]$ and $[3\bar{3}1]$.

To determine the $X(0)$ values and g-factor anisotropy $g_{[\bar{3}3\bar{1}]}/g_\perp$ and $g_{[3\bar{3}1]}/g_\perp$, the $A(\theta)/A(0)$ vs. θ data in Fig. 3(b) were fitted by Eqs. (1) and (4) with the use of $X(0)$ and $g_{[\bar{3}3\bar{1}]}/g_\perp$ (for the solid circles) and $g_{[3\bar{3}1]}/g_\perp$ (for the open ones) as the fitting parameters. The results of the best fit are shown in Fig. 3(b) by the solid curves [21]. It is seen that the data for both directions $[\bar{3}3\bar{1}]$ and $[3\bar{3}1]$ are well fitted by Eqs. (1) and (4), which allows us to obtain the Δ_s/Δ_o value for $\theta = 0$, $X(0) = 0.37 \pm 0.02$, and the values of $g_{[\bar{3}3\bar{1}]}/g_\perp$ and $g_{[3\bar{3}1]}/g_\perp$ equal to 0.6 ± 0.1 and 0.10 ± 0.05, respectively.

Thus, the above analysis shows that the ratio of the spin splitting to the orbital one for $\theta = 0$ is $X(0) = 0.37 \pm 0.02$. Therewith $g_\parallel$ depends strongly on the crystallographical directions.

Let us now compare the experimentally found value of $X(0)$ with theoretical one. To do it we calculate the energies of LLs in a magnetic field of arbitrary orientation.

IV. THE LANDAU LEVELS IN TILTED MAGNETIC FIELD

Let us choose the vector potential so that only the components lying in the plane of the quantum well are nonzero:

$$A_x = A'_x - B_y z, \quad A_y = A'_y - B_x z. \tag{5}$$

The vector potential components with strokes describe the magnetic field along the z axis:

$$H_z = \frac{\partial A'_y}{\partial x} - \frac{\partial A'_x}{\partial y}. \tag{6}$$

Let introduce creation and annihilation operators:

$$\begin{aligned} a^+ &= \frac{\lambda}{\sqrt{2}}(k_x + ik_y) = \frac{\lambda}{\sqrt{2}}k_+, \\ a &= \frac{\lambda}{\sqrt{2}}(k_x - ik_y) = \frac{\lambda}{\sqrt{2}}k_-, \end{aligned} \tag{7}$$

where

$$k_x = -i\frac{\partial}{\partial x} + \frac{eA'_x}{\hbar c}, \quad k_y = -i\frac{\partial}{\partial y} + \frac{eA'_y}{\hbar c}, \quad \lambda = \sqrt{\frac{\hbar}{|eB_z|}}. \tag{8}$$

The operators k_x and k_y satisfy the following commutation relation:

$$[k_x, k_y] = -i\frac{eB_z}{\hbar} \tag{9}$$

and therefore

$$[a, a^+] = \frac{eB_z}{|eB_z|}. \tag{10}$$

Further we supply that $B_z > 0$, so $[a, a^+] = 1$. To calculate the energy spectrum we have used the 8×8 Kane Hamiltonian which takes exactly into account interactions between the bands Γ_6, Γ_8, and Γ_7. The interactions with the other remote bands are taken into account as the second-order perturbations. An explicit form of the Hamiltonian is given in Refs. [6,22] for the quantum well grown on the (013) plane.

To incorporate the magnetic field, the following substitutions have been made:

$$k_+ \to a^+ i\frac{\sqrt{2}}{\lambda}\frac{ezB_+}{\hbar}, \quad k_- \to a\, i\frac{\sqrt{2}}{\lambda}\frac{ezB_-}{\hbar}, \tag{11}$$

where $B_\pm = B_x \pm iB_y$. Moreover, to take into account the Zeeman effect, the following term has been added to the Hamiltonian:

$$H_Z = \frac{e\hbar}{m_0}\begin{pmatrix} H_{cc} & 0 \\ 0 & H_{vv} \end{pmatrix}, \tag{12}$$

where

$$H_{cc} = \frac{1}{2}\begin{pmatrix} B_z & B_- \\ B_+ & -B_z \end{pmatrix}, \tag{13}$$

and

$$H_{vv} = \begin{bmatrix} -\frac{3\kappa}{2}B_z & -\frac{\sqrt{3}\kappa}{2}B_- & 0 & 0 & \frac{\sqrt{6}(\kappa+1)}{4}B_- & 0 \\ -\frac{\sqrt{3}\kappa}{2}B_+ & -\frac{\kappa}{2}B_z & -\kappa B_- & 0 & -\frac{(\kappa+1)}{\sqrt{2}}B_z & \frac{(\kappa+1)}{2\sqrt{2}}B_- \\ 0 & -\kappa B_+ & \frac{\kappa}{2}B_z & -\frac{\sqrt{3}\kappa}{2}B_- & -\frac{(\kappa+1)}{2\sqrt{2}}B_+ & -\frac{(\kappa+1)}{\sqrt{2}}B_z \\ 0 & 0 & -\frac{\sqrt{3}\kappa}{2}B_+ & \frac{3\kappa}{2}B_z & 0 & -\frac{\sqrt{6}(\kappa+1)}{4}B_+ \\ \frac{\sqrt{6}(\kappa+1)}{4}B_+ & -\frac{(\kappa+1)}{\sqrt{2}}B_z & -\frac{(\kappa+1)}{2\sqrt{2}}B_- & 0 & -(\kappa+\frac{1}{2})B_z & -(\kappa+\frac{1}{2})B_- \\ 0 & \frac{(\kappa+1)}{2\sqrt{2}}B_+ & -\frac{(\kappa+1)}{\sqrt{2}}B_z & -\frac{\sqrt{6}(\kappa+1)}{4}B_- & -(\kappa+\frac{1}{2})B_+ & -(\kappa+\frac{1}{2})B_z \end{bmatrix}. \tag{14}$$

In order to find the eigenvalues and eigenfunctions of the total Hamiltonian, we divided it into axially symmetric and axially asymmetric parts. On the first step we find eigenvalues and eigenfunctions of the axially symmetric part. To do it we use procedure described in Refs. [6,23]. On the second step we use these eigenfunctions as a basis for expansion of wave function of the total Hamiltonian. Then the total Hamiltonian was represented as a matrix on the basis of these eigenfunctions, which eigenvalues and eigenfunctions represent the solution of our problem. Note that eigenfunctions of the axially symmetric Hamiltonian have two quantum numbers: number of the Landau level and subband number. In expansion we usually used 30–50 Landau levels and 10–15 subbands for the calculation of electron states in our structures within the interval of magnetic field used in our experiments. Further increase of the Landau and subband numbers does not practically change the calculation results.

The parameters used in the calculations are listed in the Table II. Values for deformation potentials a_c, a_v, b, d and elastic constants C_{ij} were taken from Ref. [24]; parameter B_8 is from Ref. [25]; other parameters are from Ref. [4]. All the values were assumed linearly dependent on x excepting $E_g(x)$ which is calculated in accordance with Refs. [26,27]. The valence band offset value equal to the difference of HgTe and CdTe valence band maximum energy $E_v(\mathrm{HgTe}) - E_v(\mathrm{CdTe})$ is 570 meV [26].

An example of the Landau-level fan-chart diagram calculated for the different orientations of the magnetic field is shown in Fig. 4. It is seen that the LLs diagrams calculated for the same tilt angle θ are dependent on the orientation of $B_\parallel$ relative to the crystallographic axes. Moreover, the diagrams in Figs. 4(d) and 4(e) calculated for the two angles α distinguished by 180° are different. Thus, the Landau-level spectrum is angle dependent and exhibits the key feature analogous to that observed experimentally.

V. COMPARISON BETWEEN THEORY AND EXPERIMENT FOR $\theta = 0$

First, we have calculated the Fermi energy (E_F) which is equal to 27 meV for $n = 2.07 \times 10^{11}$ cm^{-2} that corresponds to the data represented in Figs. 2 and 3. Then we have found the cyclotron energy and the spin splitting at the energy close to the Fermi energy as the differences $\Delta_o = E_{N+2} - E_N$ and $\Delta_s = E_{2N} - E_{2N-1}$, respectively, where N is the number of the LLs numbered in a row starting with $N = 1$ [see Fig. 4(a)]. For the actual case of $n = 2.07 \times 10^{11}$ cm^{-2} and $B_\perp = 0.5$ T (see Fig. 3), the Landau levels laying close to the Fermi level have the numbers $N = 16$–18 and this estimate

TABLE II. The parameters used in the calculations.

Parameter	CdTe	HgTe
E_g (eV)	1.606	−0.303
E_v (eV)	−0.57	0
Δ (eV)	0.91	1.08
F	−0.09	0
E_p (eV)	18.8	18.8
γ_1	1.47	4.1
γ_2	−0.28	0.5
γ_3	0.03	1.3
κ	−1.31	−0.4
B_8 (eV Å^2)	−22.41	–
a (Å)	6.48	6.46
a_c (eV)	−2.925	−2.380
a_v (eV)	0	1.31
b (eV)	−1.2	−1.5
d (eV)	−5.4	−2.5
C_{11} (10^{11} din/cm^2)	5.62	5.92
C_{12} (10^{11} din/cm^2)	3.94	4.14
C_{44} (10^{11} din/cm^2)	2.06	2.19

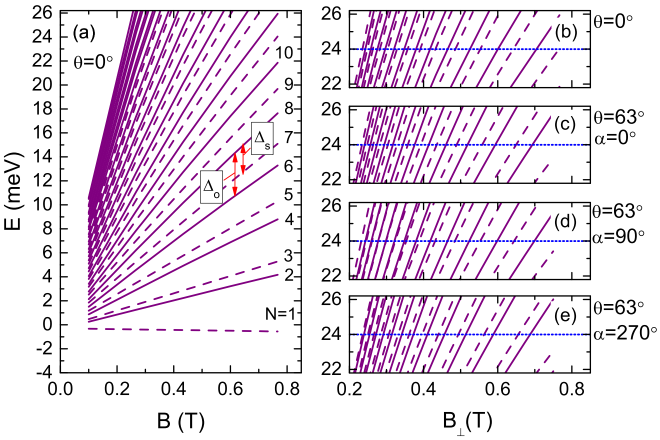

FIG. 4. (a) The Landau-level fan chart calculated for the case when the magnetic field is directed perpendicularly to the QW plane. The arrows show the orbital and spin splitting. The right panels are the Landau levels in the vicinity of the Fermi level (the dotted lines) for $n = 2.07 \times 10^{11}$ cm^{-2} at $\theta = 0^\circ$ (b) and $\theta = 63^\circ$ for $\alpha = 0^\circ$ (c), 90° (d), and 270° (e). The solid and dashed lines are related to different "spin" sublevels. The energy is measured from the bottom of the conduction band at $B = 0$.

gives $\Delta_o \simeq 2.68$ meV, $\Delta_s \simeq 1.55$ meV that corresponds to the spin-to-orbit splitting ratio $X^{\text{calc}}(0) = 0.58$. Recall that $X^{\text{exp}}(0) \simeq 0.37$ (see Sec. III). The difference between $X^{\text{calc}}(0)$ and $X^{\text{exp}}(0)$ is radical not only quantitatively but qualitatively. Really, when $X(0) > 0.5$, the different spin sublevels of the neighboring LLs with different orbital numbers should merged in low magnetic fields and the only odd minima in $\rho_{xx}(B)$ should be observed in this case. When $X(0) < 0.5$ the different spin sublevels with one and the same orbital number are merged and the only even minima in $\rho_{xx}(B)$ should be observed. As Fig. 2(c) shows, at $B_\perp < 0.7$ T we observe even minima that accords well with $X^{\text{exp}}(0) = 0.37 < 0.5$, while the theory predicts $X^{\text{calc}}(0) = 0.58 > 0.5$ which should lead to observation of the odd minima. We assume that two factors can be responsible for such a difference between $X^{\text{exp}}(0)$ and $X^{\text{calc}}(0)$. Let us consider the first one.

Experimentally, the used method gives the ratio of the spin splitting to the orbital one. The orbital splitting $\Delta_o = \hbar\omega_c = \hbar eB/m$ is determined by the effective mass at the Fermi energy. The studies of m as a function of QW width and electron density [28] show that the m value in the structure under consideration is equal to $(0.015 \pm 0.002)\, m_0$ at $n = 2.07 \times 10^{11}$ cm^{-2}, while the above calculation gives $m^{\text{calc}} = 0.0216\, m_0$ [see Fig. 5(a)]. There was supposed in Ref. [28] that such a difference between theory and experiment may result from many-body effects which are not taken into account in the theory used. If one supposes that the many-body effects lead only to decrease in the effective mass but do not change the g-factor, then one should correct the calculated value of $X^{\text{calc}}(0)$ by the following way $X^{\text{corr}}(0) = X^{\text{calc}}(0) \times m^{\text{exp}}/m^{\text{calc}} = 0.58 \times m^{\text{exp}}/m^{\text{calc}} \simeq 0.4 \pm 0.03$. As seen such a correction gives well coincidence with the experimental value $X^{\text{exp}}(0) = 0.37 \pm 0.02$.

Another reason for the difference between $X^{\text{exp}}(0)$ and $X^{\text{calc}}(0)$ may be the result of the fact that the interface inversion asymmetry was not taken into account yet in the calculation described in Sec. IV. Such a type of asymmetry is natural for the zinc-blende heterostructures due to lack of inversion symmetry in parent materials. As shown in Refs. [23,29–31] it can modify the energy spectrum significantly. To take this effect into account we used an additional term in the Hamiltonian as suggested by Ivchenko [32]. This term leads to an additional mixing of the Γ_8 and Γ_7 states at the interfaces and for the actual case can be written as follows:

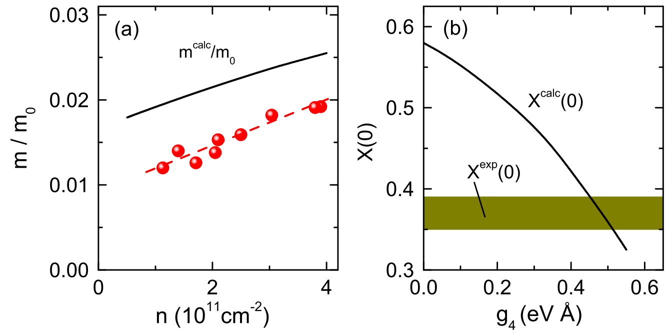

FIG. 5. (a) The calculated (solid curve) and experimental (symbols) electron density dependencies of the effective mass. The dashed line is a guide to the eye. (b) The calculated ratio of the spin splitting to orbital one $X(0)$ as a function of parameter g_4 which controls the contribution of interface inversion asymmetry.

$$H_i = \frac{dU}{dz}\frac{1}{\sqrt{3}}A_{8\times 8}, \tag{15}$$

where $A_{8\times 8}$ is a numerical matrix which explicit form is given by Eq. (5) in Ref. [23], the function $U(z)$ depends only on jump in the semiconductor composition at the boundary. As earlier we have assumed it is a linear function of the Cd content x,

$$U(z) = g_4[1 - x(z)], \tag{16}$$

where g_4 is the parameter responsible for the mixing strength. The results of the calculations are shown in Fig. 5(b), where $X^{\text{calc}}(0)$ is plotted as a function of the value of the parameter g_4. It is seen that taking into account only the interface inversion asymmetry with $g_4 = 0.45$–0.53 eV Å also gives a good agreement with the experimental value $X^{\text{exp}}(0)$. It should be noted, however, that it does not improved the agreement between theory and experiment as to the effective mass—its value only slightly depends on g_4 [28].

Thus, comparison of only $X^{\text{exp}}(0)$ with the theoretical results does not give an unambiguous answer to the question which factor, mass renormalization or interface inversion asymmetry, gives the main contribution to the difference between theory and experiment.

VI. IN-PLANE ANISOTROPY OF *g*-FACTOR, $d > d_c$

For a detailed experimental study of the in-plane anisotropy of the Zeeman splitting we measured the SdH oscillations in the configuration shown in Fig. 1(b). The rotator and the sample were set in such a way that the axis of rotation was normal to two-dimensional gas and tilted relative to the

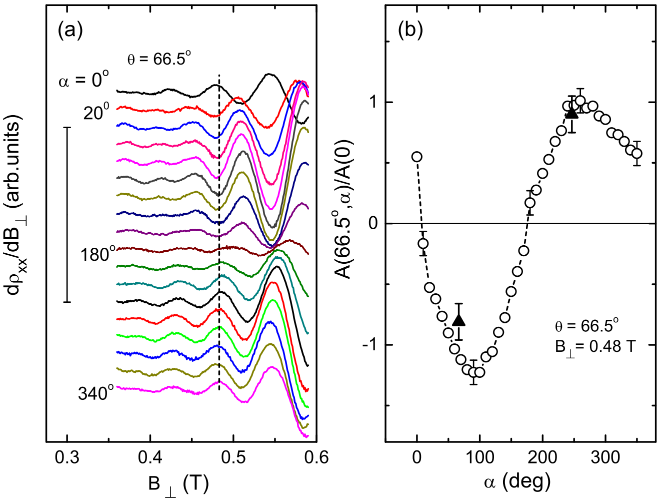

FIG. 6. (a) The $B_\perp$ dependencies of $d\rho_{xx}/dB_\perp$ for the different angles α measured at $\theta = 66.5^\circ$. (b) The normalized oscillation amplitudes $A(66.5^\circ, \alpha)/A(0)$ plotted against the angle α. The triangle shows $A(66.5^\circ, 0)/A(0)$ measured in the first configuration [see Fig. 3(b)]. The bar in panel (a) is the same as shown in Fig. 3(a).

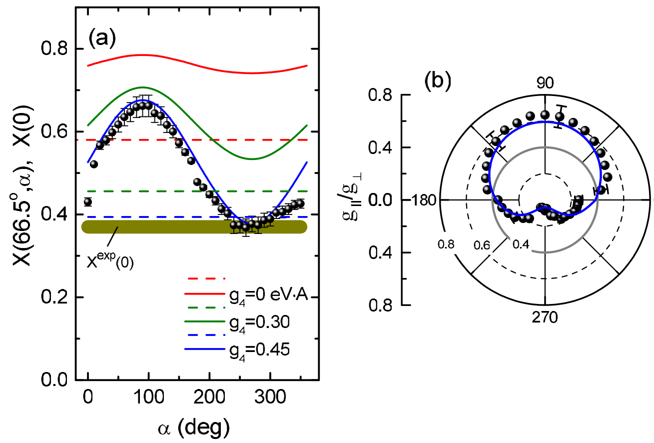

FIG. 7. (a) The ratio of the spin-to-orbit splitting for $\theta = 66.5^\circ$ plotted against the angle α. Symbols are obtained from the $A(66.5^\circ, \alpha)/A(0)$ data shown in Fig. 6(b) by using Eq. (1). The solid curves and dashed lines are the dependencies $X(66.5^\circ, \alpha)$ and the $X(0)$ values, respectively, calculated for the different values of the parameter g_4. (b) The in-plane anisotropy of g-factor, $g_\parallel(\alpha)/g_\perp$. The circles are the data, and the curve is the calculated dependence for $g_4 = 0.45$.

magnetic field by the angle θ. This angle determines the ratio of the normal to in-plane component of the magnetic field. At fixed magnetic field B, the rotation in this case changes the direction of $B_\parallel$ with respect to crystallographic axis but does not change the ratio $B_\parallel/B_\perp = \tan\theta$.

In Fig. 6(a) we represent $d\rho_{xx}/dB_\perp$ as a function of $B_\perp$ for different α at $\theta = 66.5^\circ$, where α is the angle between the $B_\parallel$ direction and the axis [100] as shown in Fig. 1(b). As seen the positions of the oscillations are practically independent of α, while the oscillation amplitudes change dramatically, so that the oscillation phases jump on π at certain angles: between $\alpha = 0^\circ$ and 20° and near $\alpha \approx 180^\circ$. The angle dependence $A(\theta = 66.5^\circ, \alpha)/A(0)$ for $B_\perp = 0.48$ T is plotted in Fig. 6(b). Using it we find from Eq. (1) the ratio of the spin splitting to the orbital one $X(66.5^\circ, \alpha)$ which is plotted against α in Fig. 7(a).

The difference between $X(66.5^\circ, \alpha)$ and X(0) can be interpreted qualitatively as the contribution of in-plane magnetic field to the spin splitting. If we assume that the effective g-factor is still described by the expression Eq. (3) even for such a complex spectrum, then we can obtain the g-factor anisotropy $g_\parallel(\alpha)/g_\perp$ as follows:

$$\frac{g_\parallel(\alpha)}{g_\perp} = \frac{1}{\tan(\theta)}\sqrt{\left[\frac{X(\theta,\alpha)}{X(0)\cos(\theta)}\right]^2 - 1}. \qquad (17)$$

The result of such a data treatment is shown in Fig. 7(b). It is seen that the in-plane g-factor extremely anisotropic. So the $g_\parallel/g_\perp$ value is close to 0.65 for $\alpha \approx 90^\circ$, while at $\alpha \approx 270^\circ$ it is equal to zero within the experimental error.

Let us compare these data with the results of theoretical calculations. In Fig. 7(a), we present the results of calculations of $X(66.5^\circ, \alpha)$ and $X(0)$ carried out for this structure for the different g_4 values. It is evident that the calculations performed without taking into account the interface inversion asymmetry, i.e., with $g_4 = 0$, give $X(66.5^\circ, \alpha)$ and $X(0)$ which significantly exceed the experimental data. Therewith the angle dependence $X(66.5^\circ, \alpha)$ is very weak, which indicates the weak anisotropy of the in-plane g-factor.

The possible reasons for the discrepancy between $X^{\text{calc}}(0)$ and $X^{\text{exp}}(0)$ were discussed in Sec. V. The first reason is associated with a smaller value of m^{exp} in comparison with m^{calc}. It was shown that taking into account the electron mass renormalization can lead to a decrease in $X^{\text{calc}}(0)$ and thus to a good agreement with $X^{\text{exp}}(0)$. Our estimates show that such accounting for the renormalization of $X^{\text{calc}}(\theta, \alpha)$ reduces the value of $X^{\text{calc}}(66.5^\circ, \alpha)$ in $m^{\text{calc}}/m^{\text{exp}}$ times also, but it does not lead to an increase in anisotropy of in-plane g-factor.

The second reason is related to the interface inversion asymmetry. The calculation of $X(66.5^\circ, \alpha)$ with taking it into account for several values of parameter g_4 are represented in Figs. 7(a) and 7(b). As clearly seen, with an increase of the parameter g_4, the calculated $X^{\text{calc}}(0)$ and $X^{\text{calc}}(66.5^\circ, \alpha)$ values become closer to the experimental ones and almost coincide with them when $g_4 = 0.45$ eV Å.

The above comparison of theoretical calculations with experimental data shows that the taking into account interface inverse asymmetry is necessary to obtain strong, comparable with experiment, anisotropy of $X^{\text{calc}}(66.5^\circ, \alpha)$. This, however, does not mean that the mass renormalization does not play any role and therefore the value $g_4 = 0.45$ eV Å obtained when only the interface inversion asymmetry is taken into account should not be considered as determined reliably.

The above results were obtained for the structure with $d = 10$ nm $> d_c$ in which the conduction band is formed from the heavy-hole states. The natural question arises: What role does the inversion of the spectrum at $d > d_c$ play in the giant anisotropy of the in-plane g-factor? To elucidate this question we turn now to analysis of the data obtained for the structure 2 with normal band ordering.

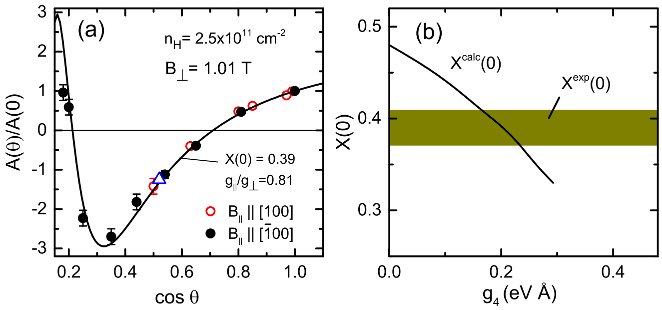

FIG. 8. (a) The dependencies of the normalized oscillation amplitude $A(\theta)/A(0)$ at $B_\perp = 1.01$ T. The symbols are the data, the curve is the dependencies calculated from Eq. (1) for $X(0) = 0.39$ and $g_\parallel/g_\perp = 0.81$. (b) The ratio of the spin splitting to orbital one $X(0)$ plotted against the g_4 value.

VII. IN-PLANE *g*-FACTOR ANISOTROPY IN THE STRUCTURE WITH $d < d_c$

To find the in-plane g-factor anisotropy in the structure with $d < d_c$ all the measurements described above were carried out for the structure 2 with $d = 4.6$ nm (see Table I). Since the analysis of the results is analogous to that described above for the structure 1 we present the key data only.

The dependence of the oscillation amplitude on the angle θ obtained in the first configuration (the rotation axis lies in the 2D plane and is perpendicular to the magnetic field) is presented in Fig. 8(a). The data shown by the open and solid circles are obtained when the in-plane B component appears in the direction [100] and [$\bar{1}$00], respectively. One can see that the angle dependencies of relative amplitude $A(\theta)/A(0)$ for both directions coincide with each other within the experimental error. The formula Eq. (1) describes well both sets of the data with the parameters $X(0) = 0.39$ and $g_\parallel/g_\perp = 0.81$. The error is estimated as ± 0.02 for both parameters.

The theoretical value of $X(0)$ calculated with neglecting the interface inversion asymmetry is equal to $X^{\rm calc}(0) = 0.46$ that is greater than 0.39 found experimentally. As discussed in Sec. V the two factors, renormalization of the effective mass and interface inversion asymmetry, can be the reasons for this discrepancy. The first factor can be excluded because, contrary to the structure 1 with $d = 10$ nm, the effective mass measured for structure 2 at $n = 2.5 \times 10^{11}$ cm^{-2} practically coincides with the calculated one: $m^{\rm exp} = (0.0225 \pm 0.002)\, m_0$, $m^{\rm calc} = 0.0222\, m_0$. As for the role of the second factor, $X^{\rm calc}(0)$ coincides with $X^{\rm exp}(0)$ when $g_4 \simeq 0.2$ eV Å [see Fig. 8(b)]. It should be noted that this value is seemingly less than that for structure 1 with $d = 10$ nm and strongly less than g_4 obtained in Ref. [23] where the valence band spectrum is investigated.

Let us inspect the data measured in the second configuration. The oscillation curves measured at $\theta = 59^\circ$ for different angles α and the α dependence of the normalized oscillation amplitude at $B_\perp = 1.01$ T are shown in Figs. 9(a) and 9(b), respectively. As seen the α dependence of the oscillation amplitude for this structure is much weaker than that for the structure 1 (see Fig. 6) that points to the relatively weak anisotropy of the in-plane g-factor directly. The last is illustrated by Fig. 10 in which the dependencies $X(59^\circ, \alpha)$ and $g_\parallel(\alpha)/g_\perp$ obtained from the data presented in Fig. 9 are shown. It is seen that the in-plane g-factor anisotropy is really weak in the structure 2 with $d < d_c$. In the same figure, the results of theoretical calculation are shown. One can see that the satisfactory agreement between theory and experiment for the angle dependencies $X(59^\circ, \alpha)$ is achieved with $g_4 = (0.1 \pm 0.05)$ eV Å.

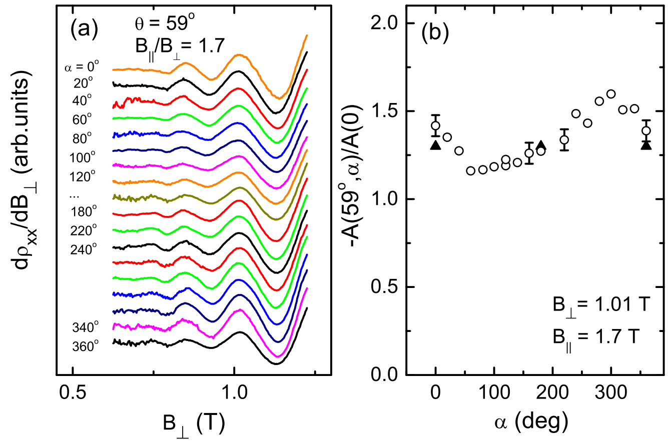

FIG. 9. (a) The $B_\perp$ dependencies of $d\rho_{xx}/dB_\perp$ for the different angles α measured for a fixed angle $\theta = 59^\circ$. (b) The normalized oscillation amplitudes $A(59^\circ, \alpha)/A(0)$ plotted against the angle α for $B_\perp = 1.01$ T. The triangle shows $A(59^\circ, 0)/A(0)$ obtained in the first configuration [see Fig. 8(a)]. Structure 2.

Before to conclude brief mention should be made of comparison between experiment and theory concerning the absolute g-factor values (Table III). In order to obtain the absolute experimental g-factor values, the experimental cyclotron effective mass was used. The theoretical values were extracted from the Landau-level fan chart at the Fermi energy corresponding to $n = 2.07 \times 10^{11}$ cm^{-2} and 2.5×10^{11} cm^{-2} with the use $g_4 = 0.45$ eV Å and 0.1 eV Å for structures 1 and 2, respectively. One can see that the theory describes the data for the structure 2 with "normal" energy spectrum satis-

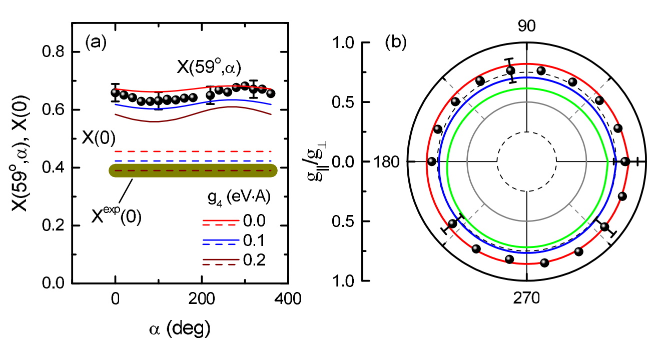

FIG. 10. (a) The ratio of the spin-to-orbit splitting for $\theta = 59^\circ$ plotted against the angle α. Symbols are obtained from the $A(59^\circ, \alpha)/A(0)$ data shown in Fig. 9(b) by using Eq. (1). The solid curves and dashed lines are the dependencies $X(59^\circ, \alpha)$ and $X(0)$, respectively, calculated for the different g_4 values. (b) The anisotropy of in-plane g-factor. The circles are the data, and the curves are the theoretical dependencies calculated with the same g_4 values as in the panel (a).

TABLE III. Effective mass and g-factor[a]: Experiment versus theory.

	Structure 1 ($d > d_c$)		Structure 2 ($d < d_c$)	
	Experiment	Theory	Experiment	Theory
$X(0)$	0.37 ± 0.02	0.37	0.39 ± 0.02	0.42
m/m_0	0.015 ± 0.002	0.0216	0.0225 ± 0.002	0.022
$g_\perp$	50 ± 3	36.1	33 ± 2	35.5
$g_\parallel^{[100]}$	16 ± 4	13.9	27 ± 3	26.6
$g_\parallel^{[\bar{1}00]}$	17 ± 2	13.9	26 ± 3	26.6
$g_\parallel^{[03\bar{1}]}$	32 ± 3	21.7	25 ± 3	25.2
$g_\parallel^{[0\bar{3}1]}$	4 ± 2	1.87	28 ± 3	27.1

[a]The absolute g-factor values are listed in the table.

factorily. As for the structure 1 with "inverted" spectrum, the discrepancy between absolute values calculated and obtained experimentally is clearly evident despite the fact that the relative values $X(\theta,\alpha)$ and $g_\parallel(\alpha)/g_\perp$ are described perfectly (see Fig. 7). Numerically, the reason for the difference between theory and experiment for g-factor is the difference in effective masses which experimental value almost one and a half times less than the theoretical one that was already discussed in Sec. V.

VIII. CONCLUSION

The Shubnikov–de Haas effect in the conduction band was investigated in the (013)-$Hg_{1-x}Cd_xTe$/HgTe quantum wells both with normal and "inverted" energy spectrum. Analyzing the oscillations measured for the different orientations of magnetic field relative to the QW plane and crystallographic directions we have obtained the anisotropy of the ratio of the spin splitting to the orbital one. The data relevant to the QWs with normal and "inverted" energy spectra differ significantly.

For the QWs with "inverted" spectrum, it has been shown that this ratio is strongly dependent both on the orientation of the magnetic field relative to the QW plane and on the orientation of the in-plane component of magnetic field relative to crystallographic axes laying in the QW plane. As for the QW with normal spectrum, this ratio being essentially dependent on the angle between the magnetic field and normal to the QW-plane reveals only weak anisotropy in the QW plane.

To interpret the data obtained, the Landau levels in the tilted magnetic field have been calculated within the framework of the four band kP model. It has been shown that the experiment results can be quantitatively described only with taking into account interface inversion asymmetry. This allows us to estimate the value of the parameter g_4 responsible for the interface inversion asymmetry contribution. It is several times smaller than that obtained for the valence band in Ref. [23]. In our opinion, this could indicate that the approximation in which the sole parameter g_4 is responsible for the interface inversion asymmetry contribution to the spectra both of conduction and valence bands is not good enough and the more accurate approach is needed.

ACKNOWLEDGMENTS

We are grateful to E. L. Ivchneko for useful discussions. The work has been supported in part by the Russian Foundation for Basic Research (Grant No. 18-02-00050), by Act 211 Government of the Russian Federation, Agreement No. 02.A03.21.0006, by the Ministry of Science and Higher Education of the Russian Federation under Project No. FEUZ-2020-0054, and by the FASO of Russia (theme "Electron" No. 01201463326).

[1] M. I. Dyakonov, *Spin Physics in Semiconductors*, Springer Series in Solid State Sciences (Springer-Verlag, Berlin, 2017).
[2] L. G. Gerchikov and A. Subashiev, Phys. Status Solidi B **160**, 443 (1990).
[3] X. C. Zhang, A. Pfeuffer-Jeschke, K. Ortner, V. Hock, H. Buhmann, C. R. Becker, and G. Landwehr, Phys. Rev. B **63**, 245305 (2001).
[4] E. G. Novik, A. Pfeuffer-Jeschke, T. Jungwirth, V. Latussek, C. R. Becker, G. Landwehr, H. Buhmann, and L. W. Molenkamp, Phys. Rev. B **72**, 035321 (2005).
[5] B. A. Bernevig, T. L. Hughes, and S.-C. Zhang, Science **314**, 1757 (2006).
[6] M. Zholudev, Ph.D. thesis, University Montpellier 2, France, 2013.
[7] I. Yahniuk, S. S. Krishtopenko, G. Grabecki, B. Jouault, C. Consejo, W. Desrat, M. Majewicz, A. M. Kadykov, K. E. Spirin, V. I. Gavrilenko, N. N. Mikhailov, S. A. Dvoretsky, D. B. But, F. Teppe, J. Wrobel, G. Cywinski, S. Kret, T. Dietl, and W. Knap, NPJ Quant. Mater. **4**, 13 (2019).
[8] S. S. Krishtopenko and F. Teppe, Phys. Rev. B **97**, 165408 (2018).
[9] X. C. Zhang, K. Ortner, A. Pfeuffer-Jeschke, C. R. Becker, and G. Landwehr, Phys. Rev. B **69**, 115340 (2004).
[10] M. Pakmehr, C. Bruene, H. Buhmann, L. W. Molenkamp, A. V. Stier, and B. D. McCombe, Phys. Rev. B **90**, 235414 (2014).
[11] M. V. Yakunin, A. V. Suslov, S. M. Podgornykh, S. A. Dvoretsky, and N. N. Mikhailov, Phys. Rev. B **85**, 245321 (2012).
[12] D. Kozlov, Z. Kvon, N. Mikhailov, and S. Dvoretsky, Pis'ma Zh. Eksp. Teor. Fiz. **100**, 824 (2014) [JETP Lett. **100**, 724 (2014)].
[13] L. S. Bovkun, S. S. Krishtopenko, M. S. Zholudev, A. V. Ikonnikov, K. E. Spirin, S. A. Dvoretskii, N. N. Mikhailov, F. Teppe, W. Knap, and V. I. Gavrilenko, Fiz. Tekh. Poluprovodn. **49**, 1676 (2015); Semiconductors **49**, 1627 (2015).
[14] N. N. Mikhailov, R. N. Smirnov, S. A. Dvoretsky, Y. G. Sidorov, V. A. Shvets, E. V. Spesivtsev, and S. V. Rykhlitski, Int. J. Nanotechnol. **3**, 120 (2006).
[15] F. F. Fang and P. J. Stiles, Phys. Rev. **174**, 823 (1968).
[16] S. A. Studenikin, P. T. Coleridge, G. Yu, and P. Poole, Semicond. Sci. Technol. **20**, 1103 (2005).
[17] G. Minkov, O. Rut, A. Sherstobitov, S. Dvoretski, and N. Mikhailov, Physica E **91**, 203 (2017).

[18] E. V. Kurganova, H. J. van Elferen, A. McCollam, L. A. Ponomarenko, K. S. Novoselov, A. Veligura, B. J. van Wees, J. C. Maan, and U. Zeitler, Phys. Rev. B **84**, 121407(R) (2011).

[19] A. Germanenko, N. Kozlova, G. Minkov, O. Rut, A. Sherstobitov, and J. Freudenberger, Physica E **42**, 960 (2010).

[20] To determine the oscillation amplitude, the experimental curves were fitted by the Lifshits-Kosevich formula [33] as described in Ref. [23].

[21] It should be noted that the $X(0)$ and $g_\parallel/g_\perp$ values can be directly obtained from the data without the fitting procedure if the experimental $A(\theta)/A(0)$ vs. θ plot has one or more extrema at some angle(-s) $\theta = \theta^\star$. As follows from Eqs. (1) and (4) the experimental values of $X(0)$ and $g_\parallel/g_\perp$ in such a case can be obtained as

$$X^{\rm exp}(0) = \frac{1}{\pi}\arccos\left[-\frac{A(0)}{A(\theta^\star)}\right]$$

and

$$\left(\frac{g_\parallel}{g_\perp}\right)^{\rm exp} = \frac{1}{(\tan\theta^\star)^2}\sqrt{\frac{1}{[X^{\rm exp}(0)]^2} - 1},$$

respectively.

[22] M. S. Zholudev, A. V. Ikonnikov, F. Teppe, M. Orlita, K. V. Maremyanin, K. E. Spirin, V. I. Gavrilenko, W. Knap, S. A. Dvoretskiy, and N. N. Mihailov, Nanosc. Res. Lett. **7**, 534 (2012).

[23] G. M. Minkov, V. Y. Aleshkin, O. E. Rut, A. A. Sherstobitov, A. V. Germanenko, S. A. Dvoretski, and N. N. Mikhailov, Phys. Rev. B **96**, 035310 (2017).

[24] K. Takita, K. Onabe, and S. Tanaka, Phys. Status Solidi B **92**, 297 (1979).

[25] R. Winkler, *Spin-orbit Coupling Effects in Two-Dimensional Electron and Hole Systems*, Springer Tracts in Modern Physics, Vol. 191 (Springer, Berlin, 2003).

[26] C. R. Becker, V. Latussek, A. Pfeuffer-Jeschke, G. Landwehr, and L. W. Molenkamp, Phys. Rev. B **62**, 10353 (2000).

[27] J. P. Laurenti, J. Camassel, A. Bouhemadou,, B. Toulouse, R. Legros, and A. Lusson, J. Appl. Phys. **67**, 6454 (1990).

[28] G. Minkov, V. Y. Aleshkin, O. Rut, A. Sherstobitov, A. V. Germanenko, S. Dvoretski, and N. Mikhailov, Physica E **116**, 113742 (2020).

[29] X. Dai, T. L. Hughes, X.-L. Qi, Z. Fang, and S.-C. Zhang, Phys. Rev. B **77**, 125319 (2008).

[30] S. A. Tarasenko, M. V. Durnev, M. O. Nestoklon, E. L. Ivchenko, J.-W. Luo, and A. Zunger, Phys. Rev. B **91**, 081302(R) (2015).

[31] G. M. Minkov, A. V. Germanenko, O. E. Rut, A. A. Sherstobitov, M. O. Nestoklon, S. A. Dvoretski, and N. N. Mikhailov, Phys. Rev. B **93**, 155304 (2016).

[32] E. Ivchenko, *Optical Spectroscopy of Semiconductor Nanostructures* (Alpha Science International, Harrow, UK, 2005), p. 427.

[33] I. M. Lifshits and A. M. Kosevich, Zh. Eksp. Teor. Fiz. **29**, 730 (1955) [Sov. Phys. JETP **2**, 636 (1956)].